UC Irvine

Title

Structures of two novel crystal forms of Aspergillus oryzae alpha amylase (taka-amylase)

Permalink

https://escholarship.org/uc/item/3nt3n0rx

Authors

Gee, Christine L
Holton, James M
McPherson, Alexander

Peer reviewed

HHS Public Access

Structures of two novel crystal forms of *Aspergillus oryzae* alpha amylase (Taka-amylase)

Christine L. Gee[1], James. M. Holton[2,3,4], Alexander McPherson[5,*]

[1]Dept. Molecular and Cell Biology and Howard Hughes Medical Institute, Stanley Hall 527, University of California, Berkeley CA 94720-3220 USA

[2]Dept. of Biochemistry and Biophysics, UC San Francisco, San Francisco, CA 94158 USA

[3]Dept. of Molecular Biophysics and Integrated Bioimaging, Advanced Light Source, MS-2108, Lawrence Berkeley National Laboratory, 1 Cyclotron Road, Berkeley, CA 94720 USA

[4]Stanford Synchrotron Radiation Lightsource, SLAC National Accelerator Laboratory, Menlo Park, CA 94025, USA

[5]Dept. Molecular Biology and Biochemistry, 3205 McGaugh Hall, University of California, Irvine, Irvine, CA 92697-3900 USA

Abstract

The structures of *Aspergillus oryzae* α-amylase were determined in a tetragonal crystal, having one molecule as asymmetric unit, and a monoclinic crystal with two molecules as asymmetric unit. Both crystal forms were obtained from trace contaminants of an old commercial lipase preparation. Structures were determined and refined to 1.65 Å and 1.43 Å resolution respectively. The latter crystal has a non-crystallographic (NCS) twofold axis within the asymmetric unit. Glycosylation at Asn197 is evident, and in the tetragonal crystal can be seen to include three, partially disordered sugar residues following the initial N-acetyl glucosamine (NAG). Superposition of the tetragonal crystal model on the α-amylases from *Bacillus subtilis* (PDB:1BAG), pig pancreas (PDB:3L2L), and barley (PDB:1AMY), show a high degree of coincidence, particularly for the $(\beta/\alpha)_8$-barrel domains, and especially within the active site. Using this structural agreement between amylases, we extrapolated the binding model of a six residue, limit dextrin found in pig pancreas α-amylase to the *Aspergillus oryzae* enzyme model, which predicts substrate interacting amino acid residues.

Keywords

glycosylation; limit dextrin; homology; substrate complex; hydration, X-ray

Introduction

α-Amylase from *Aspergillus oryzae* is a staple of the enzyme industry (1) and has been used for decades in medical and a variety of commercial processes. Taka-amylase is a typical

*amcphers@uci.edu, (831) 717-4247.

endo type amylase, and it catalyzes the hydrolysis of α-1,4-glucosidic linkages of α-1,4-glucans. It hydrolyzes amylose to maltose and glucose but is less efficient in hydrolyzing branched chain polymers of starch such as amylopectin, where activity is decreased by the production of limit dextrins. Because of its pH optimum of 4.5 it has been used even longer as a digestive aid. It is among the most active of all α-amylases (2).

Aspergillus oryzae α-amylase is a protein of M_r = 53,662 Daltons comprised of 478 amino acids, with an unusually high proportion of aromatic residues (3, 4). It has one tightly bound calcium ion (2, 5, 6, 7, 8), and it is unusual in that for the pig pancreatic enzyme it is catalytically activated by a chloride ion bound predominantly by Arg204 (9, 10, 11). X-ray crystallography has revealed that the Ca^{2+} cation, having ligands His210, Cys164 and Glu162 main chain carbonyl oxygens, as well as the side chain carboxyl of Asp175, is an integral component of the three-dimensional structure (9, 11, 12).

The protein is organized into two domains (9), a large (β/α)$_8$-barrel (13), which is responsible for at least the major part of its catalytic activity, and a small eight stranded antiparallel β-barrel, termed a carbohydrate binding domain (CBD), which is common to most polysaccharide hydrolases (14, 15). The role of the CBD in α-amylase remains, as in other hydrolases, uncertain. The enzyme from *Aspergillus oryzae* is glycosylated by a complex oligosaccharide at Asn197 (16, 17) whose exact structure remains somewhat in doubt.

Binding of substrates (11) and catalysis by α-amylases is reasonably well understood (2). There is a prominent cleft that traverses the entire face of the (β/α)$_8$-barrel, and the active site lies in a deep depression near its center. This trough is commonly referred to as the binding cleft, though it is not yet clear that every part of it participates in the binding of polymeric substrates. The catalytic center is characterized by three carboxylic acid containing residues, highly conserved among all α–amylases; those in *Aspergillus oryzae* are Asp206, Asp297 and Glu230. These conspire to hydrolyze the α-(1,4) linkage and release a maltooligosaccharide unit from the non-reducing end of the polysaccharide fragment, though, depending on the length of the substrate, the product may also be a tri- or tetra saccharide (18). The polysaccharide is associated with the enzyme in the binding cleft in large part through hydrophobic interactions with an array of aromatic residues.

α-Amylase was first crystallized from pig pancreatic juice in 1947 (19, 20) and that from *Aspergillus oryzae* in the early 1950's (21, 22). The original structure of *Aspergillus oryzae* α-amylase was determined by Matsuura, et al. (9, 23) and subsequently, α-amylases from a large variety of organisms have been determined crystallographically. One feature of α-amylases that remains somewhat of a mystery is that the enzyme is processive (18, 24, 25, 26, 27), in that it does not disengage from a glucan polymer between cleavages but continues along a polymer in sequential fashion. The source of the energy that must drive such a process remains obscure.

We have grown two crystal forms of the α-amylase from *Aspergillus oryzae* that have no entry in the PDB, though one form was reported in 1954 (21, 22, 28) but, apparently, its structure was never determined. We obtained the crystals under somewhat unusual

circumstances (see below) that we feel might be of interest to other crystallographers and serve as a caution. We have solved and refined the structures of these two crystals and report here some features of relevance to its enzymology. By extrapolation from work on pig pancreatic α-amylase, we produced a model of the enzyme with a bound limit dextrin (29, 30) of six glucose residues revealing the polypeptide components likely responsible for its binding.

Materials and Methods

Crystallization was achieved by sitting drop vapor diffusion (31, 32) in Cryschem plates (Hampton Research, Aliso Viejo, CA) containing 0.6 ml reservoirs of 12% polyethylene glycol (PEG) 3350 buffered at pH 6.5 with 0.1 M 2-(N-morpholino) ethanesulfonic acid (MES). The drops were equal amounts of a 30 mg/ml protein stock solution and the reservoir. Crystallization was at room temperature and required one to three weeks. For the structure analysis and model reported here, X-ray diffraction intensities were collected on beamline 8.3.1 at the Advanced Light Source (ALS) at the Lawrence Berkeley National Laboratory (LBNL) in Berkeley, CA using a Dectris Pilatus 6M pixel array detector. After 30 seconds to one-minute submersion in 30% 2-methyl-2,4-pentanediol (MPD) and 20% PEG 3350, the crystals were flash cooled in the cryo stream at 93 K. Relevant data and statistics for the crystals, data collection, and model refinement are shown in Table 1.

Delta-omega rotation sectors of 0.1° were collected with 0.1, 0.2, and 0.4 sec collection times. The crystals, which exhibited a mosaicity of 0.30° and diffracted to resolutions in the neighborhood of 1.5 Å, proved to be rather resistant to X-ray exposure, and were so large that two to three different volumes of a single crystal, 360° of data per site, could be recorded, providing an unusually high (33, 34) data redundancy. Data were processed and reduced as they were recorded using the program XDS. Data were scaled, reduced to an asymmetric unit, and converted to structure amplitudes using the programs POINTLESS and AIMLESS (35, 36, 37) from the CCP4 program system (38). Molecular replacement searches of the monoclinic crystal reflections were carried out using the program PHASER (39, 40, 41, 42), also from the CCP4 suite of programs (38) with PDB entry 2TAA as search model. Refinement was carried out to convergence using the program REFMAC5 (43, 44) from the CCP4 set, with final refinement using the program phenix.refine from the PHENIX suite (45). No TLS refinement (46) was used and no NCS restraints were imposed on the monoclinic crystals which contained two molecules per asymmetric unit. Isotropic displacement factors were used for both crystal forms. Graphic analysis, water addition, and most figures were generated by the program COOT (47) and Pymol (48). SDS-PAGE gels were used to determine protein components of the lipase preparation. The structures of the tetragonal and monoclinic crystals have been deposited in the Protein Data Bank and have entry codes 6XSVand 6XSJ respectively.

Results

Two crystal forms of the enzyme were grown under identical conditions, (12% PEG 3350 buffered at pH 6.5 with 0.1 M MES) both frequently appearing in the same crystallization sample. Thus, they represent classical polymorphs. Two crystal habits appeared in the

samples, tetragonal bipyramids, and polygonal blocks. The unusual circumstance noted above was that the protein stock was a commercially available *Thermomyces lanuginosa* lipase preparation provided us 20 years ago by Novo – Nordisk Co. of Copenhagen, Denmark. In other experiments we had been successful in growing a number of crystal forms of *T. lanuginose* lipase from this same preparation with identical crystallization conditions (49), and naturally expected to grow lipase crystals in these experiments. We, therefore, mistook the crystals as lipase crystals and proceeded accordingly. What came to light much later was that the lipase from *T. lanuginose* was expressed by Novo – Nordisk Company in *Aspergillus oryzae*, a common fungal expression system. Thus, *Aspergillus oryzae* proteins were produced in addition to the lipase target. While the appearance of crystals from protein impurities present in the preparation used for crystallization was, to us, unexpected, perhaps it should not have been. There are numerous instances of the occurrence, including several previously documented in the literature (50, 51).

Approximately six months and hundreds of computing hours were exhausted attempting to solve the crystal structures using molecular replacement with a wide variety of lipase models as probes. These efforts included exploring a number of possible, sometimes impossible, space groups, and assuming many kinds of twinning and disorder. No solutions, even potential solutions, could be found. This was particularly puzzling because all previous lipase crystals were readily solved using the same probes. It is our experience that when Phaser fails to solve a structure when the data and the probes are as good as we were using, then either the space group was wrong (which we had thoroughly investigated), or the protein was wrong.

A sodium dodecyl sulfate (SDS) polyacrylamide gel of the lipase preparation that yielded the crystals, Figure S1, showed a strong, major band corresponding to lipase, but another prominent band as well. Some of the minor bands were of higher molecular weight than lipase. Hence, they could not be lipase degradation products. The issue was resolved when the data for the tetragonal crystals was entered into the program SIMBAD (52). SIMBAD is a sequence-independent molecular-replacement pipeline which will firstly compare the cell with all deposited PDB entries, then if that fails, it will try MR with known contaminants and finally if the first two options failed to find a result it will then perform MR with non-redundant PDB database. After extensive search through the PDB, the program suggested that the crystals were most probably *Aspergillus oryzae* α-amylase. The SIMBAD solution was correct. Using *Aspergillus oryzae* α-amylase (2TAA) as probe, Phaser immediately found the correct solutions in both the tetragonal and monoclinic crystals. Figure 1 shows the disposition of the amylase molecules in both crystals. Ribbon tracings of the α-amylase in the tetragonal crystals are shown in Figure 1(A). The NCS twofold axis related pair that comprise the asymmetric unit of the monoclinic crystals are in Figure 1(B).

In the monoclinic crystals the NAG attached to Asn197 is very clear for both molecules in the asymmetric unit, but only one additional sugar residue of the oligosaccharide is visible, and even that, only on one of the two molecules. We have modeled that as a mannose. In the tetragonal structure several additional saccharide residues are evident, but clearly accompanied by serious disorder. We have done our best to model the density in terms of reasonable sugars (NAG-NAG-MAN-MAN), but that oligosaccharide should be viewed with

caution. Real-space correlation coefficients (RSCC) ranged from >0.9 for the initial NAG, to 0.7 for the buffers and palmitic acid (PLM), to 0.4 for the distal mannose (MAN) residues. The "twilight" scores (53) ranged from 0.8 to 0.7, indicating better than average agreement with the density when compared to other ligands in the PDB.

The alternative hypothesis of all but the most ordered NAG ligands replaced by solvent was explored by deleting these ligands and rebuilding with liberal use of partially occupied waters. The change in RSCC between the original calculated ligand density and this new, less biased, 2mFo-DFc density was smaller than 0.02 in all cases except the palmitic acids, most distal MAN, and MES, with change in RSCC 0.2, 0.1 and 0.07, respectively. This drop in RSCC indicates that these regions of the map are more susceptible to model bias than the more well-ordered regions, and that the discriminating power of the structure factor data in these regions is weak. The most likely explanation is that these moieties are partially occupied with some fraction of the density coming from partially ordered solvent, but this situation is not easily represented with contemporary models.

The covalently bound oligosaccharide, partially seen in the tetragonal crystals (Figure 2), is probably present in most, or all of the Taka-amylase crystals whose structures have been reported but was simply disordered. The electron density corresponding to the oligosaccharide we observe is accompanied by a considerable amount of confusion. In the tetragonal crystals the initial sequence of sugars, however, lies close to the surface of the protein and makes a number of close contacts. We believe these interactions, due to the molecular packing in the tetragonal unit cell, likely explain the oligosaccharide's partial appearance in the electron density. Were it not for the interactions with the protein, likely due to packing considerations, we suspect the entire oligosaccharide, with the exception of the initial NAG, would probably be disordered.

Some other ligands of interest are also present in the crystals (Figure 2), a likely consequence of the complex nature of the crystallization solutions, particularly that of the protein. Both crystal forms contained, per protein molecule, 1 MES buffer molecule. The monoclinic crystals contained two MPD and one PEG fragment (four residues) from the cryo-protective solution, and two phosphate ions. The tetragonal crystals, on the other hand, unexpectedly had two palmitic acid molecules, which might be longer, as well as the one MES buffer molecule (Figure 2). The lipids were undoubtedly acquired from the protein stock solution that was little more than the expended *Aspergillus oryzae* growth medium. It is interesting that the tetragonal crystals ($P4_12_12$) had a solvent content of 50%, about average for most protein crystals (31), while the monoclinic crystals were highly hydrated, like those from pig pancreas α-amylase, with a solvent content of 69%.

Discussion

The structure of Taka-amylase has been reported in three other crystal forms (Table 2), two of space group $P2_12_12_1$, (28) and another in space group $P2_1$ (54). The monoclinic crystal also has two molecules in the asymmetric unit related by an NCS twofold axis, but the unit cell is otherwise different than the monoclinic crystals reported here. This raises the question of what causes the polymorphism.

The general crystallization conditions for each form undoubtedly provides a partial explanation. We note, however, that the previous orthorhombic crystals were of Taka-amylase with maltose bound at the active site, and that the previous monoclinic form was Taka-amylase complexed with the inhibitor acarbose. Furthermore, (see below) our tetragonal crystals contained two ordered molecules of palmitic acid (likely nutrients in the lipase preparation used for crystallization) and a molecule of the crystallization buffer, MES.

We suggest that this array of amylase crystal forms further points up the oversize influence of conventional, small molecules in facilitating macromolecular crystal growth. Indeed, this observation has been exploited in some depth (55, 56, 57) and supported by numerous follow-on studies (58, 59, 60). Those small molecules include not only enzymologically relevant ligands such as maltose and acarbose in the case of Taka-amylase, but unanticipated ligands such as palmitic acid and MES.

Some years ago, we solved and described the structure of pig pancreatic α-amylase in complex with an extended limit dextrin (11, 61, 62, 63). It was of interest to us to investigate the structural similarity of the amylase from *Aspergillus oryzae* with the pig pancreas enzyme (PDB entry 3L2L). In addition, we included the α-amylase from the bacterial *Bacillus subtilis*, whose structure (64) is also known and extensively studied (PDB entry 1BAG), and the amylase from a plant, barley (PDB entry 1AMY (65)). Evolutionarily, the enzymes should be distant from one another, being that they represent three different taxonomic kingdoms. Superposition of the proteins indicated that the major secondary structural features of the three alpha / beta barrels superimposed very well, but that the loops connecting the elements did not match well in space. The three enzymes from *Aspergillus oryzae*, *Bacillus subtilis*, and pig pancreas were trimmed of protruding loops where there was significant disagreement with any one of the others. The three cores used in a further analysis are described in Table 3 and visual representations presented in Figure 3.

Superposition of the cores of the three molecules produced the alignment shown in Figure 3, with rms coordinate deviations found in Table 3. The large $(\beta/\alpha)_8$-barrel domains, which, presumably, contain all of the catalytic machinery of the enzyme, were independently superimposed as well, and the statistics also shown in Table 3. All of the amylases contain, in addition to the catalytic $(\beta/\alpha)_8$-barrel domains, a small domain of about 100 amino acids forming a compact antiparallel beta barrel (the CBD). The small domains of the three proteins were also independently superimposed as well, and the statistics also shown in Table 3.

Separately, the structure of a plant α-amylase, that from barley (1AMY), was similarly trimmed of most loops and it, and its individual large and small domains, superimposed upon the trimmed structures of the α-amylase from pig (3L2L). As shown in Table 3, $(\beta/\alpha)_8$-barrel domains of the two superimposed with significantly lower rms deviations in alpha carbons than for any other pairing, but the small domains exhibited much higher rms deviations between the two alpha carbon chains than any other pairing. Therefore, the $(\beta/\alpha)_8$-barrel domains of α-amylases from higher plants and animals are much more similar with one another in structure than with the protein from microorganisms. Rather unexpectedly, however, the small domains are far more dissimilar. This is speculation, but

the primary substrate in animals is glycogen, while in plants it is starch, and this may be reflected in the differences in the small domains. Indeed, there is some evidence that the function of the small domains of α-amylase is to interact with the extended substrates and prepare them for hydrolysis, hence their name, Carbohydrate Binding Domains, or CBD (14, 66).

Given the striking agreement between the three dimensional structures of the enzymes from widely different sources, the conservation of amino acid residues, and the almost exact superposition of the enzyme active site regions, we considered the possibility of extrapolating limit dextrin binding results from the pig pancreas α-amylase model (3L2L) (11) to the enzyme from *Aspergillus oryzae*. The model of pig pancreas α-amylase (3L2L) contains maltopentose bound at the active site of the enzyme as well as an additional glucose residue α-1,6-linked at the 3-glucose residue. Because active site clefts of pig pancreas α-amylase and *Aspergillus oryzae* amylase are virtually superimposable, we believed it reasonable to place the six glucose residues of the limit dextrin at the active site of *Aspergillus* α-amylase as in the pig enzyme. This, then, would allow inspection of its environment to determine what amino acid residues might be involved in its binding in the fungal enzyme. Figure 4 illustrates that arrangement.

Table 4 is an accounting of what amino acids of the *Aspergillus* α-amylase are potentially in contact with or proximal to each of the sugar residues in the oligomer. The conformations of side chains in the ligand free enzyme would almost certainly be different in the actual presence of limit dextrin. The major impediment to the binding of limit dextrin is the flexible loop composed of amino acids 168 – 172. That loop would have to move to another position in order for the limit dextrin to be accommodated as in the pig enzyme. Indeed, there is a major difference in the length and disposition of that loop between the two enzyme species. In the pig pancreas enzyme, the corresponding loop is very short and compact, while in the *Aspergillus oryzae* amylase it is large and extended. Among the interacting residues are the three catalytic residues Asp206, Asp297, and Glu230 from the *Aspergillus* enzyme, which superimpose precisely on the corresponding amino acids Asp197, Asp300 and Glu233 of the pancreatic enzyme (11, 12). Figure 4(a) shows the disposition of these three residues with respect to the bound oligosaccharide.

Supplementary Material

Refer to Web version on PubMed Central for supplementary material.

Acknowledgements

References

1. Ichishima E: Development of enzyme technology for *Aspergillus* oryzae, A. sojae, and A. luchuensis, the national microorganisms of Japan., Biosci. Biotechnol. Biochem, 80, 1681–1692 (2016). [PubMed: 27151561]

2. Yamamoto T: Handbook of Amylases and Related Enzymes: Their Sources, Isolation, Methods, Properties and Applications., The Amylase Research Society of Japan, 284 (1988).

3. Toda H, Kondo K, and Narita K: The Complete Amino Acid Sequence of Taka-amylase A., Proc. Japan Acad, 58B, 208–2123 (1982).

4. Tada S, Iimura Y, Gomi K, Takahashi K, Kara S, and Yoshizawa K: Cloning and Nucleotide Sequence of the Genomic Taka-amylase A Gene of *Aspergillus oryzae.*, Agr. Biol. Chem, 53, 593–599 (1989).

5. Muus J, Brockett FP, and Connelly CC: The effect of various ions on the stability of crystalline salivary amylase in solution., Arch. Biochem. Biophys, 65, 268–274 (1956). [PubMed: 13373424]

6. Vallee BL, Stein EA, Sumerwell WN, and Fischer EH: Metal content of alpha-amylases of various origins, J. Biol. Chem, 234, 2901–2905 (1959). [PubMed: 13840892]

7. Thoma JA, Spradlin JE, and Dygert S: Plant and Animal Amylases, pp. 115–189, in: Boyer PD and Lardy M (Ed.), The Enzymes, vol.5. Academic Press, NY (1971).

8. Fischer E and Stein E: Alpha Amylases, The Enzymes, 4, 313 (1960).

9. Matsuura Y, Kusunoki M, Harada W, and Kakudo M: Structure and possible catalytic residues of Taka-amylase A., J. Biochem, 95, 697–702 (1984). [PubMed: 6609921]

10. Levitzki A and Steer ML: The allosteric activation of mammalian alpha-amylase by chloride, Eur. J. Biochem, 41, 171–180 (1974). [PubMed: 4856205]

11. Larson SB, Day JS, and McPherson A: X-ray crystallographic analyses of pig pancreatic alpha-amylase with limit dextrin, oligosaccharide, and alpha-cyclodextrin., Biochemistry, 49, 3101–3115 (2010). [PubMed: 20222716]

12. Larson SB, Greenwood A, Cascio D, Day J, and McPherson A: Refined molecular structure of pig pancreatic alpha-amylase at 2.1 Å resolution., J. Mol. Biol, 235, 1560–1584 (1994). [PubMed: 8107092]

13. Ollis DL, Cheah E, Cygler M, Dijkstra B, Frolow F, Franken SM, Harel M, Remington SJ, Silman I, Schrag J, and other XXX authors: The α/β hydrolase fold., Protein Eng, 5, 197–211 (1992). [PubMed: 1409539]

14. Boraston AB, Bolam DN, Gilbert HJ, and Davies GJ: Carbohydrate-binding modules: fine-tuning polysaccharide recognition., Biochem. J, 382, 769–781 (2004). [PubMed: 15214846]

15. Wilkens C, Svensson B, and Moller MS: Functional Roles of Starch Binding Domains and Surface Binding Sites in Enzymes Involved in Starch Biosynthesis, Frontiers in plant science, 9, 1652 (2018). [PubMed: 30483298]

16. Yamaguchi H, Ikenaka T, and Matsushima Y: The complete sequence of a glycopeptide obtained from Taka-amylase A., J. Biochem, 70, 587–594 (1971). [PubMed: 5134660]

17. Saita M, Ikenaka T, and Matsushima Y: Isolation and characterization of -D-mannosidase from soy bean., J. Biochem, 70, 827–833 (1971). [PubMed: 5169172]

18. Robyt JF and French D: Multiple attack and polarity of action of porcine pancreatic alpha-amylase., Arch. Biochem. Biophys, 138, 662–670 (1970). [PubMed: 5464796]

19. Meyer KH, Fischer EH, and Bernfeld P: Crystallization de l'α- amylase de pancreas., Experientia, 3, 106 (1947).

20. McPherson A and Rich A: X-ray crystallographic analysis of swine pancreas amylase, Biochim. Biophys. Acta, 285, 493–497 (1972). [PubMed: 4633645]

21. Akabori S, Hagihara B, and Ikenaka T: Purification and crystallization of Taka-amylase., Proc. Jpn. Acad. Ser. B, 27, 350–351 (1951).

22. Akabori S, Ikenaka T, and Hagihara B: Isolation of crystalline taka- amylase A from "Takadiastase Sankyo"., J. Biochem, 41, 577–582 (1954).

23. Matsuura Y, Kusunoki M, Harada W, Tanaka N, Iga Y, Yasuoka N, Toda H, Narita K, and Kakudo M: Molecular structure of taka-amylase A. I. Backbone chain folding at 3 Å resolution, J. Biochem, 87, 1555–1558 (1980). [PubMed: 6156152]

24. Breyer WA and Matthews BW: A structural basis for processivity, Protein Sci, 10, 1699–1711 (2001). [PubMed: 11514661]

25. Zheng F and Ding S: Processivity and Enzymatic Mode of a Glycoside Hydrolase Family 5 Endoglucanase from Volvariella volvacea., Appl. Environ. Microbiol, 79, 989–996 (2013). [PubMed: 23204424]

26. Robyt JF and French D: Multiple attach hypothesis of alpha-amylase action: action of porcine pancreatic, human salivary, and *Aspergillus* oryzae alpha-amylases., Arch Biochem. Biophys, 122, 8–16 (1967). [PubMed: 6076229]

27. Robyt JF and French D: The action pattern of porcine pancreatic alpha-amylase in relationship to the substrate binding site of the enzyme., J. Biol. Chem, 245, 3917–3927 (1970). [PubMed: 5531189]

28. Vujicic-Zagar A and Dijkstra BW: Monoclinic crystal form of *Aspergillus* niger alpha amylase in complex with maltose at 1.8 A resolution., Acta. Cryst. F, 62, 716–721 (2006).

29. Loyter A and Schramm M: The glycogen - amylase complex as a means of obtaining highly purified alpha-amylases, J. Biol. Chem, 241, 2611–2617 (1962).

30. Loyter A and Schramm M: Multimolecular complexes of alpha-amylase with glycogen limit dextrin., Biochem. Biophys. Acta, 65, 200 206 (1966).

31. McPherson A: Crystallization of Biological Macromolecules. Cold Spring Harbor Laboratory Press, Cold Spring Harbor, NY (1999).

32. McPherson A: The Preparation and Analysis of Protein Crystals. John Wiley and Sons, New York (1982).

33. Kabsch W: Integration, scaling, space-group assignment and post-refinement, Acta Cryst. D, 66, 133–144 (2010). [PubMed: 20124693]

34. Kabsch W: Xds, Acta Cryst. D, 66, 125–132 (2010). [PubMed: 20124692]

35. Evans PR: Scaling and assessment of data quality., Acta Cryst. D, 62, 72–82 (2006). [PubMed: 16369096]

36. Evans PR: An introduction to data reduction: space-group determination, scaling and intensity statistics, Acta Cryst. D, 67, 282–292 (2011). [PubMed: 21460446]

37. Evans PR and Murshudov GN: How good are my data and what is the resolution?, Acta Cryst. D, 69, 1204–1214 (2013). [PubMed: 23793146]

38. Bailey SM: The CCP4 Suite - Programs for Protein Crystallography., Acta Cryst, D50, 760–763 (1994).

39. Read RJ: Pushing the boundaries of molecular replacement with maximum likelihood., Acta Cryst, D57, 1373–1382 (2001).

40. Storoni LC, McCoy AJ, and Read RJ: Likelihood-enhanced fast rotation functions, Acta Cryst. D 60, 432–438 (2004). [PubMed: 14993666]

41. McCoy AJ, Grosse-Kunstleve RW, Adams PD, Winn MD, Storoni LC, and Read RJ: Phaser crystallographic software, J Appl. Cryst, 40, 658–674 (2007). [PubMed: 19461840]

42. McCoy AJ, Grosse-Kunstleve RW, Storoni LC, and Read RJ: Likelihood-enhanced fast translation functions, Acta Cryst. D 61, 458–464 (2005). [PubMed: 15805601]

43. Murshudov GN, Skubak P, Lebedev AA, Pannu NS, Steiner RA, Nicholls RA, Winn MD, Long F, and Vagin AA: REFMAC5 for the refinement of macromolecular crystals., Acta Cryst., D67, 355–367 (2011).

44. Murshudov GN, Vagin AA, and Dodson EJ: Refinement of macromolecular structures by the maximum-likelihood method, Acta Cryst. D, 53, 240–255 (1997). [PubMed: 15299926]

45. Afonine PV, Grosse-Kunstleve RW, Echols N, Headd JJ, Moriarty NW, Mustyakimov M, Terwilliger TC, Urzhumtsev A, Zwart PH, and Adams PD: Towards automated crystallographic structure refinement with phenix.refine, Acta Cryst. D, 68, 352–367 (2012). [PubMed: 22505256]

46. Winn W, Isupov M, and Murshudov GN: Use of TLS parameters to model anisotropic displacements in macromolecular refinement., Acta Cryst. D, 57, 122–133 (2001). [PubMed: 11134934]

47. Emsley P and Cowtan K: COOT model - building tools for molecular graphics., Acta Cryst. D, 60, 2126–2132 (2004). [PubMed: 15572765]

48. DeLano WL: The PyMOL Molecular Graphics System, DeLano Scientific (2002).

49. McPherson A, Larson SB, and Kalasky A: The Crystal Structures of Thermomyces (Humicola) Lanuginosa Lipase in Complex with Enzymatic Reactants, Current Enzyme Inhibition, 16, 1–15 (2020).

50. Gai Z, Nakamura A, Tanaka Y, Hirano N, Tanaka I, and Yao M: Crystal structure analysis, overexpression and refolding behaviour of a DING protein with single mutation, Journal of synchrotron radiation, 20, 854–858 (2013). [PubMed: 24121327]

51. Morales R, Berna A, Carpentier P, Contreras-Martel C, Renault F, Nicodeme M, Chesne-Seck ML, Bernier F, Dupuy J, Schaeffer C, and other XXX authors: Serendipitous discovery and X-ray structure of a human phosphate binding apolipoprotein, Structure, 14, 601–609 (2006). [PubMed: 16531243]

52. Simpkin AJ, Simkovic F, Thomas JMH, Savko M, Lebedev A, Uski V, Ballard C, Wojdyr M, Wu R, Sanishvili R, and other XXX authors: SIMBAD: a sequence-independent molecular-replacement pipeline, Acta Cryst. D 74, 595–605 (2018).

53. Weichenberger CX, Pozharski E, and Rupp B: Visualizing ligand molecules in twilight electron density, Acta Crystallographica Section F, 69, 195–200 (2013).

54. Brzozowski AM and Davies GJ: Structure of Aspergillus oryzae α - amylase complexed with the inhibitor acarbose at 2.0 Å resolution., Biochem, 36, 10837–10845 (1997). [PubMed: 9283074]

55. McPherson A and Cudney B: Searching for silver bullets: an alternative strategy for crystallizing macromolecules, J Struct Biol, 156, 387–406 (2006). [PubMed: 17101277]

56. Larson SB, Day JS, Cudney R, and McPherson A: A Novel Strategy for the Crystallization of Proteins: X-ray Diffraction Validation., Acta Cryst D, 63, 310–318 (2007). [PubMed: 17327668]

57. McPherson A, Nguyen C, Larson SB, Day JS, and Cudney R: Development of an alternative approach to protein crystallization, Journal of structural and functional genomics, 24, 1803–8192 (2007).

58. Larson SB, Day JS, Nguyen C, Cudney B, and McPherson A: Progress in the Development of an Alternative Approach to Macromolecular Crystallization., Crystal Growth and Design 8, 3038–3052 (2008).

59. McPherson A, Nguyen C, Cudney R, and Larson SB: The role of small molecule additives and chemical modification in protein crystallization., Crystal Growth and Design, 1, 11, 1469–1474 (2011).

60. McPherson A, Day J, and Larson SB: Lattice Interactions in Crystals of Soybean Trypsin Inhibitor (Kunitz) Produced by Inclusion of 1,5-Disulfonylnaphthlalene., Crystal growth & design, 19, 2963–2969 (2019).

61. Heller J and Schramm M: Alpha-amylase limit dextrin's of high molecular weight obtained from glycogen Biochem Biophys, 81, 96–103 (1964).

62. Leloup VM, Colonna P, and Marchis-Mouren G: Mechanism of the adsorption of pancreatic alpha-amylase onto starch crystallites, Carbohydr Res, 232, 367–374 (1992). [PubMed: 1423363]

63. Levitski A, Heller J, and Schramm M: Specific precipitation of enzyme by its substrate. The alpha amylase - macrodextrin complex., Biochem Biophys Acta, 81, 101 (1964).

64. Fugimoto Z, Mizuno H, Takase K, and Doui N: Alpha amylase from Bacillus Subtilis complexed with maltopentose., J. Mol. Biol, 277, 393–407 (1998). [PubMed: 9514750]

65. Kadziola A, Abe J, Svensson B, and Haser R: Crystal and molecular structure of barley alpha-amylase, J. Mol. Biol, 239, 104–121 (1994). [PubMed: 8196040]

66. Paldi T, Levy I, and Shoseyov O: Glucoamylase starch-binding domain of *Aspergillus* niger B1: molecular cloning and functional characterization, Biochem J, 372, 905–910 (2003). [PubMed: 12646045]
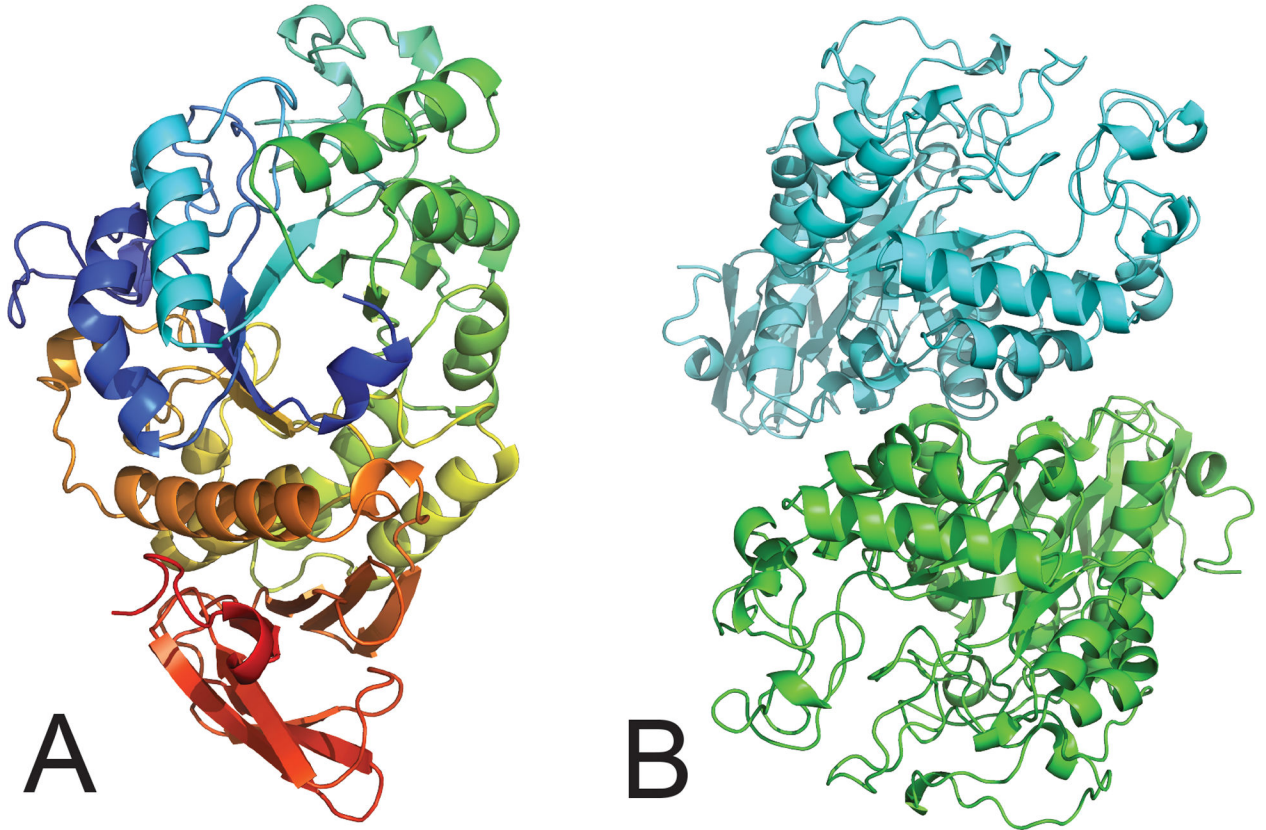
Fig 1.

In (A) is a schematic drawing of *Aspergillus oryzae* α-amylase based on the model derived from the tetragonal crystal form. In (B) are the two molecules of *Aspergillus oryzae* α-amylase comprising the asymmetric unit of the monoclinic crystals, oriented so that the NCS dyad is perpendicular to the plane of the figure.
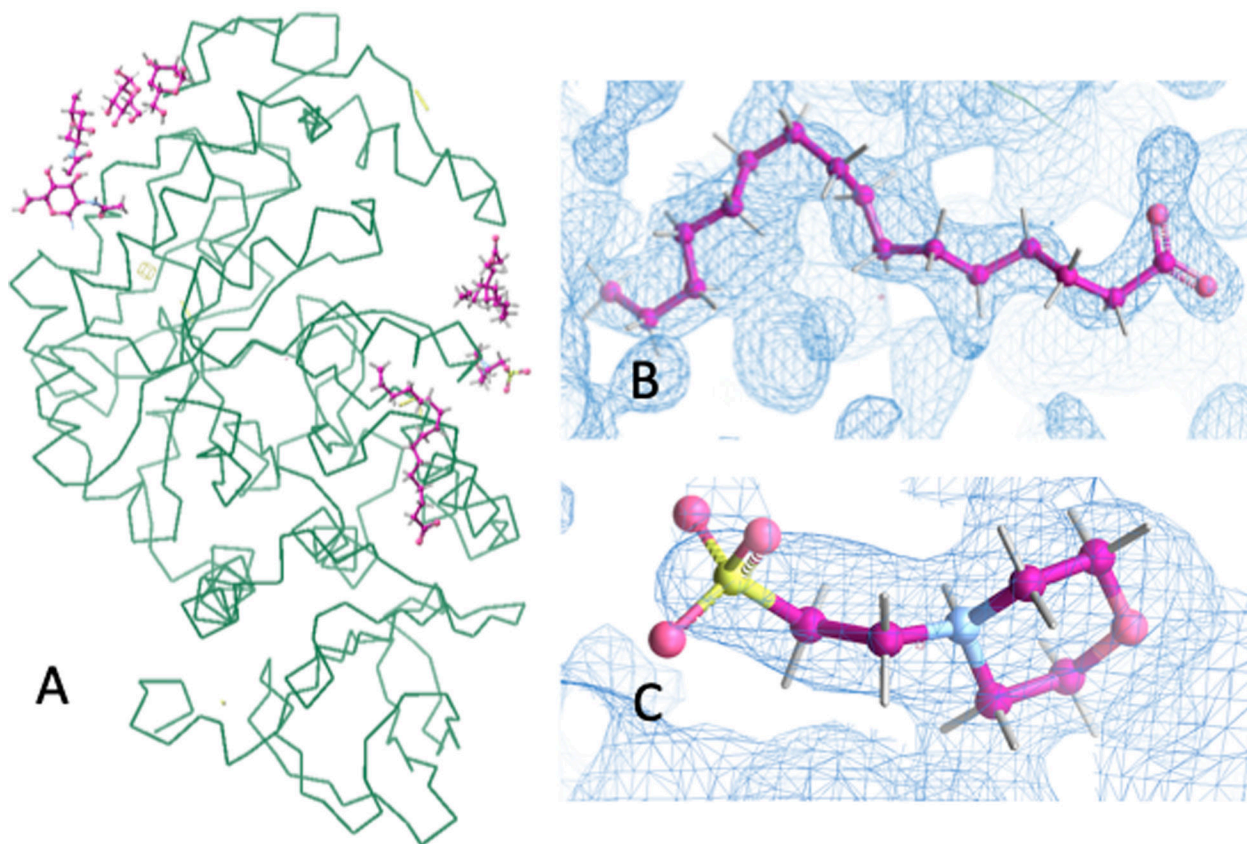
Fig 2.
In (A) is a Cα tracing of Taka-amylase from the tetragonal crystals (in green) with the two palmitic acid, MES, and covalently bound oligosaccharide (in pink) in stick and ball representation. In (B) is a stick representation of one palmitic acid on its corresponding $2F_o$ $-F_c$ electron density, and in (C) the MES molecule. If the palmitic acids and the MES are excluded from model refinement (PHENIX – REFINE) all appear strongly in $F_o - F_c$ difference Fourier omit maps.
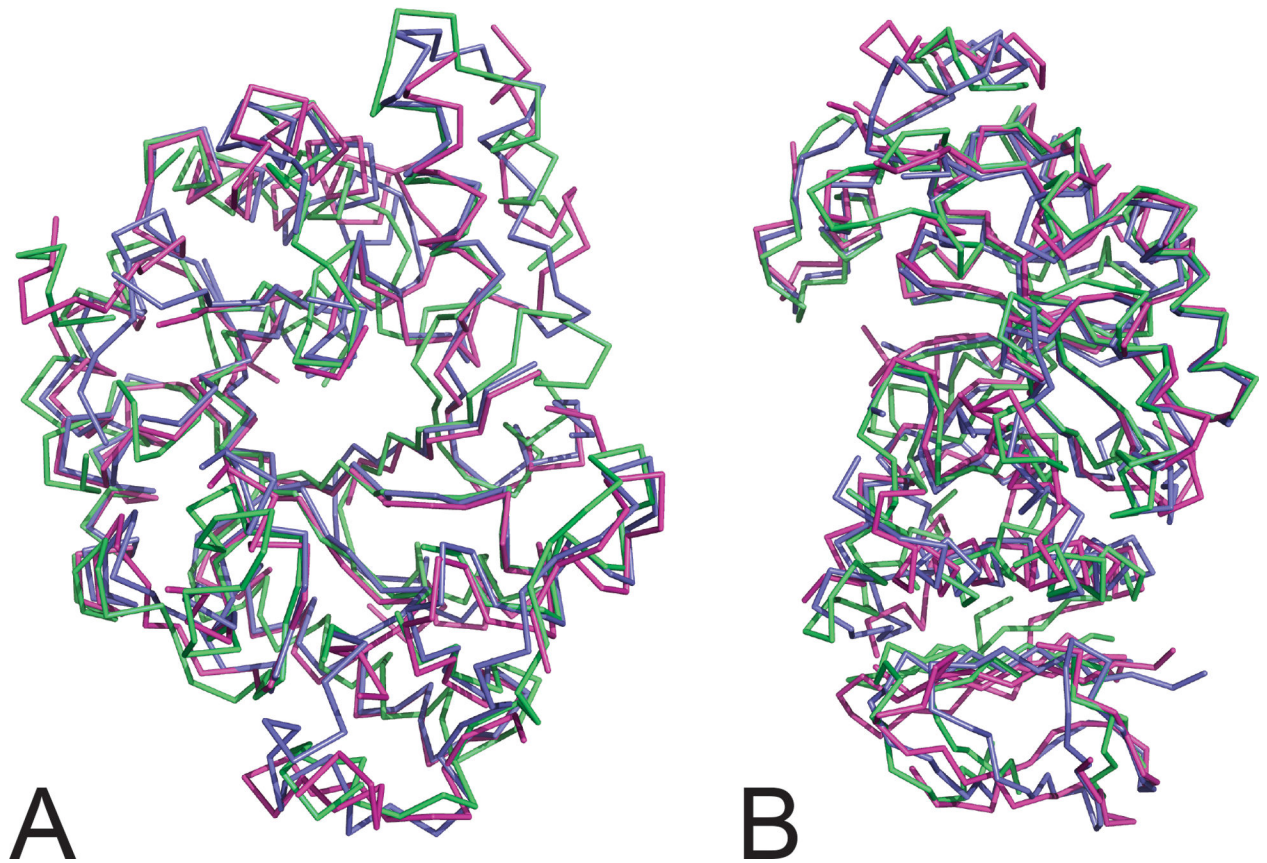
Fig 3.
In (A) the cores of the α-amylases from *Aspergillus oryzae*, *Bacillus subtilis*, and pig pancreas $(\beta/\alpha)_8$-barrels, with conflicting loops removed, are shown superimposed and to be virtually congruent. Peptides of *Aspergillus oryzae* α-amylase are in green, those of *B. subtilis* in purple, and those from pig pancreas α-amylase are in blue. In (B) the entire molecules $((\beta/\alpha)_8$-barrel and CBD domains) from the same three organisms are shown superimposed, again illustrating the remarkable similarities in the three-dimensional structures.
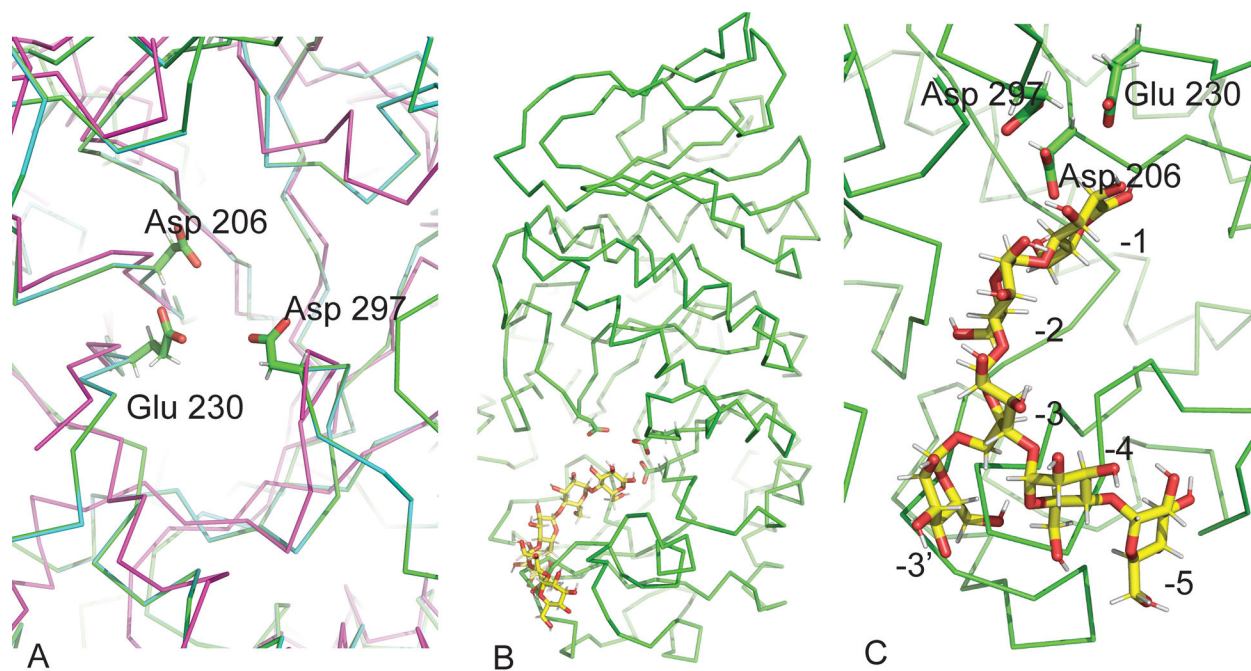
Fig 4.

In (A) the α-amylases from *Aspergillus oryzae* and pig pancreas were superimposed with the catalytic residues Asp297, Asp206 and Glu230 from *Aspergillus* on the corresponding Asp300, Asp197 and Glu233 of pig pancreas. The alignment was completely consistent with the overall superposition of the core domains ($\beta/\alpha)_8$-barrels) of the two enzymes. Using these coincident orientations, the limit dextrin of six glucose residues (11), (PDB entry 3L2L), was transferred from the pig pancreatic α-amylase to the *Aspergillus oryzae* α-amylase. The limit dextrin is shown in (B) as it might be bound to the *Aspergillus oryzae* α-amylase. In (C) is a detail of the limit dextrin as it is positioned with respect to the catalytic residues. From the placement of the limit dextrin on the *Aspergillus oryzae* α-amylase the residues potentially responsible for limit dextrin binding were deduced.

Table 1.

Crystal data, reflection processing and model refinement statistics

Crystal	Monoclinic	Tetragonal
X-ray source	ALS beamline 8.3.1	ALS beamline 8.3.1
Detector	Dectris Pilatus 6M pixel	Dectris Pilatus 6M pixel
Wavelength (Å)	1.116	1.116
Resolution range (Å)	76.7 – 1.43 (1.45 – 1.43)	66.45 – 1.65 (1.68 – 1.65)
Space group	$P2_1$	$P4_12_12$
Cell dimensions		
a, b, c (Å)	76.93, 89.94, 123.42,	63.13, 63.13, 265.81
α, β, γ (°)	90, 94.49, 90	90, 90, 90
V_M (Å^3) /Da- % solvent	3.97 – 69%	2.47 – 50.2%
Total no. reflections	5,994,500 (200,50)	8210,172 (127,117)
Unique reflections	307,462 (15,076)	66,065 (3,098)
R_{merge}	0.158 (0.740)	0.162 (0.880)
R_{meas}	0.163 (0.560)	0.159 (0.910)
R_{pim}	0.036 (0.341)	0.027 (0.462)
Completeness (%)	99.7 (98.8)	99.8 (96.8)
Multiplicity	19.5 (13.3)	124.3 (41.0)
CC1/2	0.998 (0.98)	0.999 (0.489)
Mean I/sig(I)	9.1 (0.4)	16.7 (1.1)
Wilson B (Å^2)	28.0	22.0
Refinement		
Resolution (Å)	63.18 – 1.43 (1.45 – 1.43)	61.42 – 1.65 (1.709 – 1.65)
No. reflections	156796 (8258)	65929 (6328)
R_{work} / R_{free}	0.2180/0.2508 (0.4306/0.4191)	0.175/0.204 (0.347 /0.350)
No. atoms	8760	4321
Protein	7396	3709
Ligand/ion	105	98
Water	1259	514
B-factor overall (Å^2)	19.17	39.89
B-factor Protein (Å^2)	17.03	38.53
B-factor Ligands/ions (Å^2)	50.65	69.83
B-factor Waters (Å^2)	29.17	43.96
R.m.s. Bond length dev. (Å)	0.012	0.010
R.m.s. Bond angle dev. (°)	1.04	1.10
Ramachandran favored (%)	97.68	96.62
Ramachandran allowed (%)	2.32	3.38
Ramachandran outliers (%)	0.00	0.00

Crystal	Monoclinic	Tetragonal
Rotamer outliers (%)	1.25	0.5
Clashscore	3.63	4.58

Table 2.

Comparison of Taka-amylase models from different crystal forms

	Cell dimensions (Å, °)	Ligands	Crystallization conditions	RMSD Cα atoms (Å)	PDB code
$P4_12_12$	a = b = 63.1 c = 265.8 $\alpha = \beta = \gamma = 90$	Ca^{2+}, N-glycosylation on Asn 197, MES, Palmitate	12% PEG 3350, 0.1 M MES pH 6.5	Reference structure	6XSV (This study)
$P2_1$	A = 64.99, b = 95.19, c = 74.99 $\alpha = \gamma = 90$, $\beta = 103.5$	Ca^{2+}, N-glycosylation on Asn 197, MES, phosphate, MPD, PEG	12% PEG 3350, 0.1 M MES pH 6.5	A 0.4260 475 residues B 0.2220 475 residues	6XSJ (This study)
$P2_1$	a = 91.9, b = 133.3, c = 94.3 $\alpha = \gamma = 90$, $\beta = 102.7$	Ca^{2+}	8 to 11 % protein in 0.05 M Tris-HCl pH 7.2, 2 mM $CaCl_2$, 2M ammonium sulfate.	A 1.4122 B 1.4093 C 1.4089 430 residues	2TAA
$P2_12_12_1$	a = 50.9, b = 67.2, c = 132.7 $\alpha = \beta = \gamma = 90$	Ca^{2+}	Drop: 30 mg/ml protein in 50 mM Na acetate, pH 6.0, 2 mM CaC12, 8% (w/v) PEG 8000 reservoir: 16% PEG 8000 50 mM Na acetate, pH 6.0, 2 mM $CaCl_2$	0.2549 476 residues	6TAA
$P2_12_12_1$	a = 50.8, b = 67.1, c = 131.6 $\alpha = \beta = \gamma = 90$	Ca^{2+}, Modified acarbose hexasaccharide $C_{37}H_{63}NO_{26}$	18% MM PEG 5000, 5mM $CaCl_2$, 0.1M HEPES, PH 7.5	0.3779 476 residues	7TAA
$P2_12_12$	a = 102.8, b = 63.2, c = 74.5, $\alpha = \beta = \gamma = 90$	Ca^{2+}, N-glycosylation on Asn 197	30% PEG 8000, 0.2M Na-acetate, 0.1M Na-cacodylate, pH 6.8,	0.2549 476 residues	2GUY
$P2_1$	a = 65.5, b = 101.1, c = 75.2, $\alpha = \gamma = 90$, $\beta = 103.9$	Ca^{2+}, N-glycosylation on Asn 197, alpha maltose, beta maltose	30% PEG 6000, 0.1M ammonium sulphate, 0.1M MES, pH 6.5	A 0.1955 476 residues B 0.3508 475 residues	2GVY

Table 3 -

Superposition of (b/a)$_8$-Barrel (Large) and CBD (Small) Domains

Superposition	Ref. residues	Moving residues	Aligned residues	gaps	rmsd Å	% seq. identity
1BAG / 6XSV	357	363	251	23	2.47	19.9
3L2L / 6XSV	357	379	284	19	2.63	20.8
3L2L / 1BAG	363	379	297	16	2.20	22.6
1BAG / 6XSV large dom.	296	306	218	15	2.04	23.4
3L2L / 6XSV large dom.	296	307	227	17	2.02	23.3
3L2L / 1BAG large dom.	306	307	246	15	2.20	21.5
1BAG / 6XSV small dom.	61	57	43	4	2.01	11.6
3L2L / 6XSV small dom.	67	76	42	5	3.30	9.52
3L2L / 1BAG small dom.	57	76	32	2	3.42	3.12
1AMY / 3L2L	496	403	302	19	2.26	17.54
1AMY / 3L2L large dom.	307	262	227	17	1.52	20.7
1AMY / 3L2L small dom.	76	51	37	8	3.50	8.1

6XSV: *A. oryzae* α-amylase, 1BAG: *B. subtilis* α-amylase, 3L2L: pig pancreas α-amylase, 1AMY: barley α-amylase

Table 4. -

Limit Dextrin Interactions with *Aspergillus oryzae* α - Amylase

Glucose Residue	Interactions with amino acids
1	Tyr 155, Lys 209, Leu 232
2	His 210, Leu 166, Leu 232, Thr 207, Glu 230
3	Asp 297, His 296, Leu 166, Tyr 82, Asp 206, His 122
4	Leu 173, Trp 83, His 80
5	Tyr 75, Gly 167
6	Tyr 125, Asp 126, Thr 73, Tyr 75, Tyr 83, Leu 60, Gly 127